JOURNAL OF GUIDANCE, CONTROL, AND DYNAMICS
Vol. 15, No. 6, November-December 1992

Experimental Results of Active Control on a Large Structure to Suppress Vibration

H. J. Dunn*
NASA Langley Research Center, Hampton, Virginia 23681

The need to suppress vibration in large space structures is a continuing problem during design. Active control of structural vibration is one method that can be used to achieve lightweight structures with desirable damping characteristics. In this paper three design methods, linear quadratic Gaussian with loop transfer recovery, H_∞, and μ synthesis, are used to obtain compensators for suppressing the vibrations of a 10-bay vertical truss structure, a component typical of what may be used to build a large space structure. For the design process the plant dynamic characteristics of the structure were determined experimentally using an identification method. The resulting compensators were implemented on a digital computer and tested for their ability to suppress the first bending mode response of the 10-bay vertical truss. For these experiments, the first bending mode is excited and the control system is used to damp the vibration. Time histories of the measured motion are presented, and modal damping obtained during the experiments is compared with analytical predictions. The advantages and disadvantages of using the various design methods are discussed.

Nomenclature

A,B,C,D = coefficients of dynamic equation of motion
$G(z)$ = transfer function, discrete z transform
$g(s)$ = transfer function, continuous s transform
J = performance index
K_f = LQR feedback gain matrix
K_q = LQG/LTR gain matrix
K_∞ = H_∞ compensator
Q,R = LQR weighting matrices
$r,r(s)$ = output of a compensator or plant
S = sensitivity function
s = Laplace transform variable s, $F(s)=\int_0^\infty e^{-st}f(t)\,dt$
t = time, s
$u,u(s)$ = input to the compensator or plant
W_1,W_2 = sensitivity function weighting matrices
W_{add} = additional uncertainty used in μ compensator design
W_{unc} = input uncertainty used in μ compensator design
x = state vector
z = transform variable z, $F(z)=\Sigma_{n=0}^{\infty}f(n\Delta t)z^{-n}$, also $z=e^{j\omega\Delta t}$
Υ = LQG/LTR process distribution matrix
Δt = sampling interval, s
$\mathcal{E}$ = expectation function
ζ = critical damping ratio
η,ξ = LQG/LTR white noise processes design methods
ω = frequency

Introduction

WITHIN the last decade, much attention has been focused on the active and passive control of structures to suppress their structural vibrations. Spacecraft that require accurate pointing are sensitive to the low-frequency flexible structural modes that result from minimizing weight in spacecraft designs. Active control methods can be used to damp out undesirable structural vibration while still maintaining low spacecraft weight.

A series of active control compensators, designed with linear quadratic Gaussian (LQG) with loop transfer recovery (LTR), H_∞, and μ synthesis methods, were tested in the NASA Langley Spacecraft Dynamics Laboratory to investigate the use of active control methods to suppress spacecraft structural vibration. In addition to the relative performance of the designed compensators, the robustness properties of the compensators were investigated. The compensators were tested on a 10-bay truss that is typical of what may be used to build a large space structure. The truss is vertically mounted, clamped at the top, and controlled by two pneumatic proportional thrusters that are mounted at its bottom. This paper describes the truss structure, the compensator design procedures, and the analytical and experimental results obtained from the derived compensators.

Experimental 10-Bay Truss Structure

The control laws were tested on a 10-bay truss structure (Fig. 1) located in the NASA Langley Spacecraft Dynamics Laboratory. The aluminum truss, vertically mounted and clamped at the top, is 100 in. long with a square cross section of 10 in. × 10 in. The first two natural vibration modes have been identified as 5.8 and 7.3 Hz by Juang et al.[1] using the eigensystem realization algorithm (ERA) method. The 5.8 Hz motion of the truss is in the plane defined by the truss and the force vector of the thrusters and will be referred to as the in-plane mode. The 7.3 Hz motion of the truss is in the plane perpendicular to the in-plane mode plane and will be referred to as the out-of-plane mode. Three accelerometers aligned with the principal axes of the truss are located at the bottom of the truss.

Two pneumatic proportional thrusters attached to each side of the last bay are configured such that a positive command to both thrusters produces a torque about the vertical axis of the truss. Therefore, the thrusters can be modulated either asymmetrically, to produce a force in the plane of the truss and the force vector, or symmetrically, to produce a torque about the longitudinal axis of the truss. Each thruster can generate up to 2.2 lb of force and has an approximate transfer function of $g(s)=62/(s+294)$ lbf/V.

Received June 26, 1991; presented as Paper 91-2692 at the AIAA Guidance, Navigation, and Control Conference, New Orleans, LA, Aug. 12-14, 1991; revision received Feb. 11, 1992; accepted for publication Feb. 28, 1992.

*Aerospace Engineer, Aeroservoelasticity Branch, Structural Dynamics Division.

Table 1 Zeros, poles, gain, and margins for the LQR/LTR compensators, $\mathcal{E}(\eta^2) = 0.01$

				Margin			
ρ	Z_i	P_i	K	G_{ARX}, dB	P_{ARX}, deg	G_{ERA}, dB	P_{ERA}, deg
10	−5950 −222	(−0.0816, 36.8)	−6.36e−5	49	—	12/−15	25/−98
10^2	−3790.0 −3790.0	(−0.119, 37.0)	−4.05e−4	37	142/−123	−5	56
10^3	882 −577	(−0.241, 38.4)	0.00330	28	110/−109	−36	66
10^4	−2070 120	(−0.498, 47.5)	0.0223	23	108/−107	−36	102/−95
10^5	2780 48.5	(−0.687, 78.7)	−0.114	20	107/−108	−31	−30

The control laws are implemented using a personal computer with a 80386 processor and 80387 coprocessor running a real-time Unix operating system (UNIX is a trademark of AT&T). The control laws are programmed in the C language and use floating point arithmetic for all control law calculations. The data acquisition system uses 12-bit analog-to-digital and digital-to-analog converters with a sampling rate of 200 Hz. The electrical interface provides the buffering and amplifiers required such that for a 10-V signal the thrusters generate a 2.2 lbf, and a 1 g acceleration produces a 5-V signal.

Compensator Design

The goal of these experiments was to obtain data for validating the performance of various compensators that were designed to enhance the damping characteristics of the 10-bay truss structure. An arbitrary design specification is set to just increase the critical damping ratio ζ of the in-plane bending mode (i.e., the 5.8-Hz mode) using asymmetrical control inputs. By using this simple design specification, the focus of results of this paper was shifted to the properties of the difference compensator designs. These properties are characteristic to the design methods and independent of the complexity of the plant being controlled.

Design Model

A system identification procedure instead of a finite element method was used to identify the model transfer function for use in the design procedure. The autoregressive with extra input, or ARX, model and the system identification procedure described by Ljung[2,3] were chosen because of their simple form and ease of use. Although there exists system identification procedures that are more accurate, such as the ERA method, the resulting ARX model allows for the investigation of the effects of model uncertainties on the resulting compensator designs.

The transfer function obtained using the ARX model is

$$G(z) = z^{-n_k} \frac{b_0 + b_1 z^{-1} + \cdots + b_{n_b-1} z^{-n_b}}{1 + a_1 z^{-1} + \cdots + a_{n_a} z^{-n_a}}$$

where z is the delay operator $z^{-1} = e^{-j\omega\Delta t}$, $j\omega$ is the complex frequency, and Δt is the sampling interval. The input parameters n_a, n_b, and n_k describe the order of the ARX model and hereafter will be referred to as an $[n_a, n_b, n_k]$ ARX model. The input disturbance u used in the identification algorithm consists of a constant-magnitude signal with the sign of the disturbance the same as the sign of a unit variance normally distributed random sequence as described by Ljung.[3]

To prevent higher-order modes from corrupting the estimate of the plant, the accelerations are filtered before applying the ARX procedure with the following:

$$y_n = 0.0675x_n + 0.1349x_{n-1} + 0.0675x_{n-2} + 1.143y_{n-1} - 0.4128y_{n-3}$$

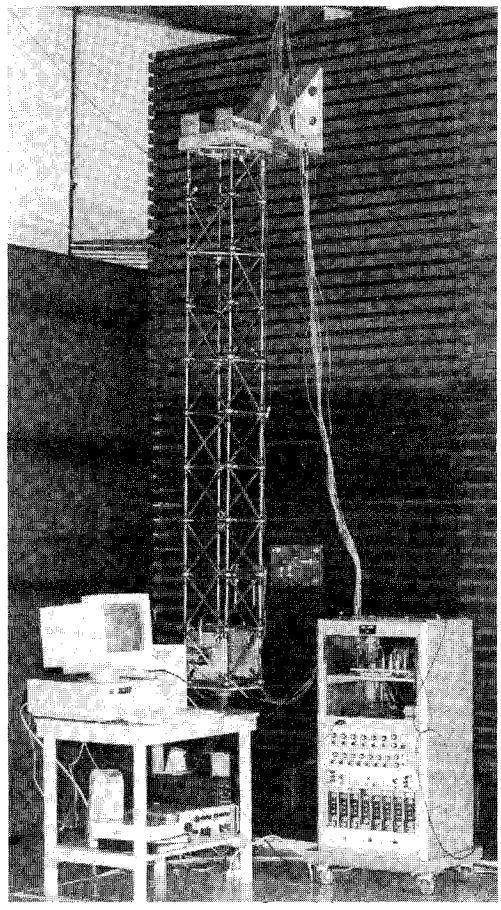

Fig. 1 Ten-bay truss structure.

which is a 10-Hz second-order Butterworth filter for a sampling rate of 20 Hz. The resulting filtered sequence is reversed and run back through the same filter. The resulting sequence is equivalent to filtering the original sequence with a 10-Hz zero-phase fourth-order Butterworth filter. By using a zero-phase filter, the need for including this filter in the compensator implementation is eliminated.

To minimize the complexity of the resulting compensator, the smallest possible design model is preferred. Therefore, a [4, 2, 4] ARX model was identified as the optimal ARX model order during model validation. The standard deviation of the residual of this model for the entire sample of 2000 data points is 0.001 V. This is sufficiently small, when compared with the 0.005 V quantization error of the data acquisition system, to obtain a good estimation of the plant. The estimated plant dynamics then were transformed into the following dynamic equations:

$$\dot{x} = Ax + Bu$$
$$r = Cx + Du$$

Table 2 Zeros, poles, gain, and margins for the LQR/LTR compensators, $\varepsilon(\eta^2)=0.0025$

				Margin			
ρ	Z_i	P_i	K	G_{ARX}, dB	P_{ARX}, deg	G_{ERA}, dB	P_{ERA}, deg
10	−3050 −243	(−0.110, 36.9)	−1.72e−4	48	—	5/−17	16/−100
10^2	2540 −255	(−0.148, 37.1)	0.00100	34	126/−128	−7	57
10^3	636 −507	(−0.269, 38.7)	0.00780	26	101/−101	−38	69
10^4	−1575 110	(−0.529, 48.8)	0.0489	20	99/−98	−38	114/−70
10^5	2000 47.3	(−0.691, 82.1)	−0.250	17	98/−100	−34	−28

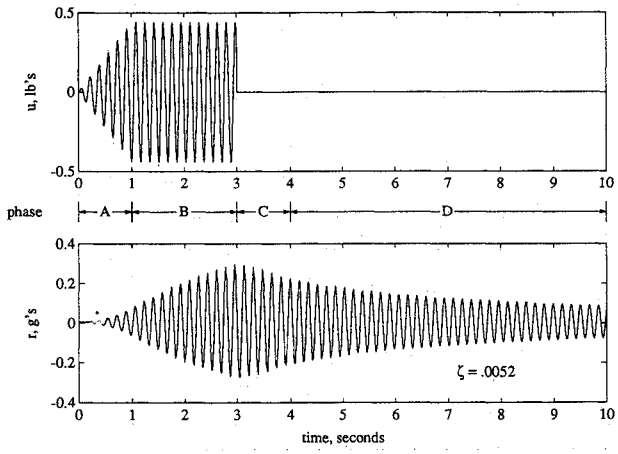

Fig. 2 Experimental results for open-loop in-plane response.

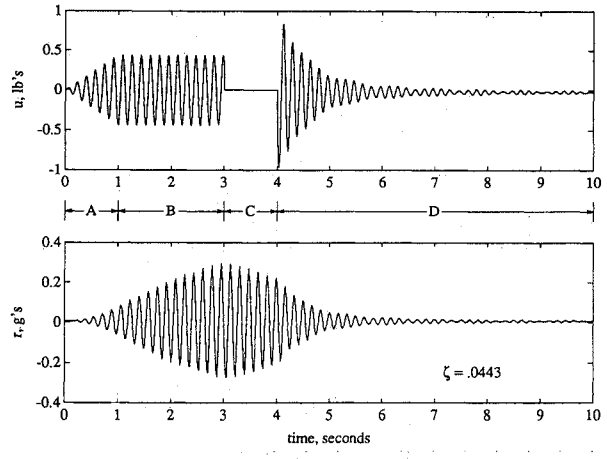

Fig. 3 Experimental results for LQG/LTR system, $\rho=10^4$.

where

$$A=\begin{bmatrix} -15.58 & 62.72 & 0 & 0 \\ -62.72 & -15.58 & 0 & 0 \\ 0 & 0 & -0.5963 & 36.68 \\ 0 & 0 & -36.68 & -0.5963 \end{bmatrix}$$

$$B=\begin{bmatrix} -1.241 \\ -0.7003 \\ -0.1209 \\ -0.4292 \end{bmatrix}$$

$$C=\begin{pmatrix} -0.05545 & 0.4075 & 2.127 & -1.102 \end{pmatrix} \qquad D=(0)$$

This plant estimate has two slightly damped poles at 5.8 and 10.3 Hz, a complex zero at 89 Hz, with $\zeta=0.86$, and a real zero at $-441\ s^{-1}$. Note that this estimate of the plant is not in total agreement with the estimate of the plant dynamics presented by Juang et al.[1] The out-of-plane bending mode has been identified using the ARX method as 10.3 Hz or 3 Hz higher than the ERA model. This plant estimate was accepted for use as a design model because of its small size and a known perturbation from the actual plant. By designing compensators with this design model, the relative strength and weakness of each of the design methods can be explored with respect to this perturbation.

Open- and Closed-Loop Test Procedures

The open-loop plant and each closed-loop system were tested by applying a test signal to the truss structure for 10 s. The test signal is composed of four phases, as shown in Fig. 2: 1) forced oscillation ramp-up (A); 2) forced oscillation at constant amplitude (B); 3) free decay (C); and 4) active control (D). In phase A, a sinusoidal input is applied to the thrusters at a frequency of 5.8 Hz. This signal, initially of zero amplitude, is linearly increased in 1 s to provide a maximum thrust equal to 0.44 lbf. The amplitude of the sinusoidal signal is held constant for 2 s during phase B, and in phase C, the structure is allowed to vibrate freely for 1 s. To reduce the distortion of the output response by the initial transient response caused by engaging the compensator, the compensator input is engaged while leaving the compensator output open during phase C. During phase D, the compensator output loop is closed, allowing the compensator to damp the structural vibrations.

Open-Loop Test Results

The four test signal phases are shown in Fig. 2, in which the system input and output response for the open-loop case also are shown. The estimate of the critical damping ratio ζ is calculated using the ERA method by assuming the acceleration data in phase D to be the output response due to an impulse. Using this procedure, the value of the critical damping ratio for the open-loop case is calculated to be 0.0052.

LQG/LTR Compensator Design

The LQG/LTR compensator design is used in this report to provide a basis of comparison for the other compensator designs. The LQG/LTR design was not optimized to produce the maximum performance. The design is a simple compensator that does a reasonable job of adding damping to the structure to suppress vibration.

LQR Compensator Design

The LQR full-state feedback compensators were designed to minimize the performance index

$$J=\int_0^\infty \left(x'Qx+\frac{1}{\rho}u'Ru\right)dt$$

Table 3 Zeros, poles, gain, and margins of H_∞ compensators

				Margin			
ρ	Z_i	P_i	K	G_{ARX}, dB	P_{ARX}, deg	G_{ERA}, dB	P_{ERA}, deg
0.0001	3980	(−0.117, 37.0)	−0.0010	28	88/−88	−12	40
	258	(−0.0209, 36.7)					
	(−0.0230, 36.7)						
0.0005	534	(−0.279, 38.5)	−0.0312	19	75/−75	−45	74
	(−0.0271, 36.8)	(−0.0244, 36.8)					
	−363						
0.001	−427	(−0.406, 41.1)	−0.119	15	73/−73	−47	92/−113
	250	(−0.0320, 36.1)					
	(−0.0357, 37.0)						
0.002	−800	(−0.608, 50.1)	−0.359	11	73/−68	−48	−63
	103	(−0.065, 37.4)					
	(−0.073, 37.7)						
0.003	618	(−0.563, 59.4)	0.680	9	68/−65	−47	−10
	111	(−0.195, 44.4)					
	(−0.161, 46.1)						
0.004	920	(−0.453, 58.5)	0.774	8	69/−62	−49	−18
	80.1	(−0.319, 55.5)					
	(−0.181, 53.5)						
0.005	1280	(−0.295, 66.5)	0.825	7	70/−59	−50	−30
	(−0.191, 56.4)	(−0.482, 54.7)					
	63.0						

Table 4 Zeros, poles, gain, and margins of μ no. 1 compensators

				Margin			
ρ	Z_i	P_i	K	G_{ARX}, dB	P_{ARX}, deg	G_{ERA}, dB	P_{ERA}, deg
0.09	−44.6	−0.288	−0.0358	62	—	—	—
		−1.162					
0.19	−352	−0.357	0.103	50	—	17/−8	38
	11.8	−1.24					
	−11.3	(−0.0437, 36.7)					
0.38	−188	−0.628	0.618	43	—	6/−19	38
	−17.6	−1.78					
	12.5	(−0.0590, 36.7)					
0.75	−214	−0.803	37.8	24	110/−87	−37	43
	−13.6	−6.06					
	0.425	(−0.704, 36.1)					
1.50	2.49	−1.22	−6.44	27	105/−84	−36	19
	(−0.852, 39.5)	−7.51					
		(−0.430, 33.2)					
3.0	65.1	−1.14	−157	12	95/−83	−24	138/−40
	16.1	(−0.729, 40.9)					

where ρ is the design parameter described by Harvey et al.[4] Simply stated, as ρ is increased, the magnitude of the compensator gain is increased, resulting in improved performance. Solving the appropriate Riccati equation, the full-state feedback gains K_f are found. The weighting matrices Q and R were chosen so that J is the square of the velocity of the in-plane bending mode plus the square of the control input. This causes the damping of the in-plane bending mode to increase from $\zeta = 0.025$ at $\rho = 10$ to $\zeta = 0.664$ at $\rho = 10^5$, whereas the root of the out-of-plane bending mode is left unchanged for the same variation in ρ.

LQG/LTR Estimator Design

Since the LQR compensator designs require the values of the state vector x to be implemented, an LQG/LTR state estimator is constructed for each of the LQR designs. The LQG/LTR procedure used in this research follows the methods presented by Doyle and Stein.[5,6] The dynamic equations used for the LQG/LTR procedure are

$$\dot{x} = Ax + Bu + \Upsilon\xi$$

$$r = Cx + Du + \eta$$

where A, B, C, and D are the plant system quadruple matrices that are used for the LQR compensator designs, and ξ and η are white noise processes with expectations $\mathcal{E}$ of

$$\mathcal{E}(\xi) = 0 \qquad \mathcal{E}(\xi^2) = 0.1$$

$$\mathcal{E}(\eta) = 0 \qquad \mathcal{E}(\eta^2) = 0.01$$

The process distribution matrix Υ is set to the control input matrix B, consistent with the LTR procedure for recovering the robustness properties of the LQR compensator at the input of the plant. The LQG/LTR gains K_q are found by solving the appropriate Riccati equation. Table 1 shows the zeros, poles, and gain of the five LQG/LTR compensator designs for various values of ρ. Note that for the complex poles listed in Table 1 (ζ, ω_N) denote the roots of ($\zeta\omega_N \pm \omega_N\sqrt{1-\zeta^2}\,j$). The transfer function for the parameters given in Table 1 is

$$\frac{r(s)}{u(s)} = K\frac{\Sigma s - Z_i}{\Sigma s - P_i}$$

Table 1 also lists the gain and phase margins calculated using the ARX plant model (G_{ARX}, P_{ARX}) and the ERA plant model (G_{ERA}, P_{ERA}). The LQG/LTR compensators recover a minimum of ±6 dB gain and ±60 deg phase margin from the LQR design when the margins are calculated with the ARX plant model. When the margins are calculated with the ERA plant model, the margins of the LQR design are not recovered.

LQG/LTR Test Results

A typical input signal and experimental response of the LQG/LTR system for a value of ρ of 10^4 is presented in Fig. 3. The input u is the same as for the open-loop case except for the closed-loop response in phase D. For a compensator designed with values of $\rho < 10^4$, the closed-loop damping of the output response is proportional to the value of ρ. However, for a compensator designed with values of $\rho > 10^4$, there is little change in the damping of the in-plane mode. The maximum damping ratio of the in-plane bending mode for this series of compensators is 0.0443. The performance of the closed-loop system can be increased by changing $\mathcal{E}(\eta^2)$ to 0.0025 in the LQG/LTR design. The maximum damping ratio of the in-plane bending mode for this series of compensators is 0.1019. However, the characteristics of the roots of the closed-loop system for changes in the value of ρ were unchanged. The zeros, poles, gain, and margins of the compensator are given in Table 2.

Figure 4 shows the results of a root locus analysis for the in-plane and out-of-plane modes. The analysis was done using the design model, i.e., ARX design model, and the ERA identified model for the plant. The behavior of the root locus for the ARX plant model is as expected; the in-plane bending root moves to the left until it meets a zero formed from poles of the compensator. The out-of-plane mode, not shown in Fig. 4, remains unchanged. The root locus using the ERA model for the plant indicates reduced damping for the in-plane mode and an unstable out-of-plane mode for $\rho > 115$. It is of interest to note that neither the ARX plane model nor the ERA plant model predict the closed-loop behavior of the LQG/LTR compensators. However, the ERA model has the correct trend in that if higher performance compensators were tested, then the out-of-plane mode instability would have been evident.

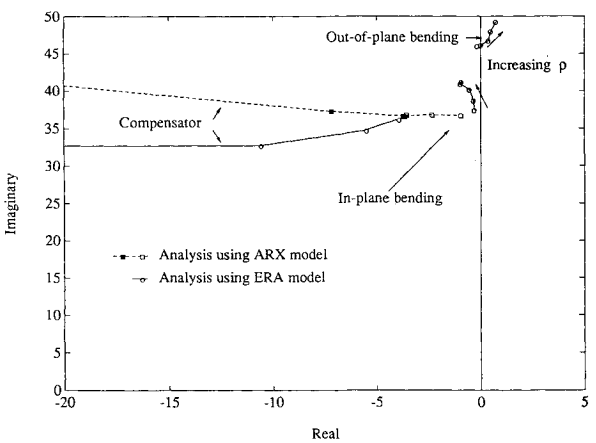

Fig. 4 Analytical root locus of closed-loop LQG/LTR system.

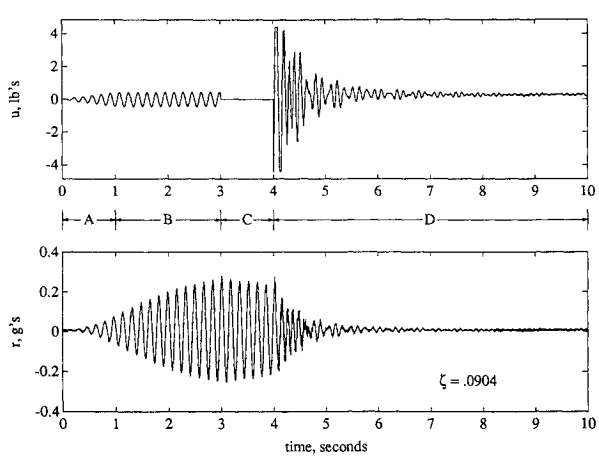

Fig. 5 Experimental results for H_∞ design with $\rho = 0.003$.

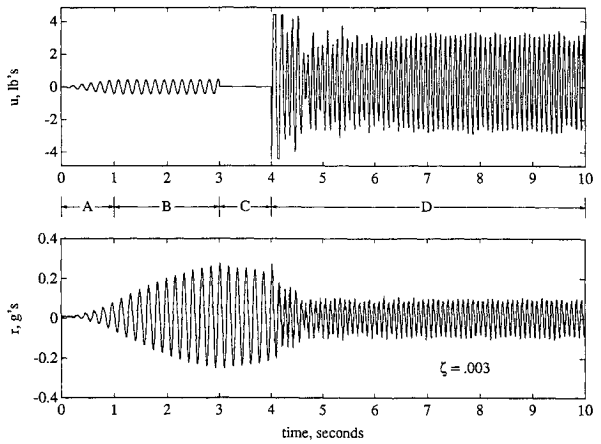

Fig. 6 Experimental results for H_∞ design with $\rho = 0.004$.

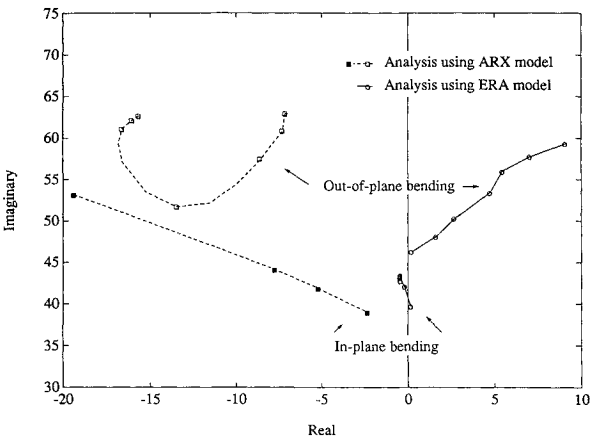

Fig. 7 Root locus analysis for H_∞ design.

H_∞ Compensator Design and Results

The H_∞ design model is identical to the model used by Francis et al.[7] The design variables are the transfer functions W_1 and W_2 defined by

$$X(s) = W_1(s)S(s)W_2(s)$$

where S is the sensitivity function of the closed-loop system to changes in the plant

$$S(s) = \left[I + P(s)K_\infty(s)\right]^{-1}$$

The H_∞ compensator minimizes the H_∞ norm of X, i.e., the supremum over ω of the largest singular value of $X(j\omega)$. The procedure used to find K_∞ is presented by Doyle et al.[8] The transfer function W_1 is chosen to excite the variables to be attenuated. For the design problem used in this research, W_1 was chosen to be unity. The transfer function W_2 was found by trial and error such that the resulting frequency response of the compensator is flat until the roll-off frequency. The W_2 is described by

$$W_2 = \rho \frac{37^2}{s^2 + 2(0.0204)37s + 37^2}$$

where ρ is now the design parameter for the H_∞ design method. The parameter ρ in W_2 has the same effect on the compensator design as did the ρ in the LQR compensator design, i.e., increasing ρ results in increased performance by increasing the magnitude of $X(s)$. The supremum of the largest singular value for all of the H_∞ compensators designed for the research are less than 0.02. The zeros, poles, gain, and margins of the H_∞ compensators designed are given in Table 3.

Table 5 Zeros, poles, gain, and margins of μ no. 2 compensators

				Margin			
ρ	Z_i	P_i	K	G_{ARX}, dB	P_{ARX}, deg	G_{ERA}, dB	P_{ERA}, deg
0.0031	124	(−0.132, 39.5)	−20.7	13	81/−61	−17	116
0.0063	105	(−0.161, 41.1)	−36.2	11	79/−66	−26	126
0.0125	65.7	(−0.224, 44.5)	−85.6	10	87/−73	−52	147/−44
0.0250	51.0	(−0.348, 51.0)	−202	10	92/−75	−48	165/−29
0.0500	41.9	(−0.483, 61.3)	−449	10	92/−78	−47	−30
0.1000	37.0	(−0.546, 71.0)	−800	8.8	90/−77	−46	−36

Table 6 Zeros, poles, gain, and margins of μ no. 3 compensators

				Margin			
ρ	Z_i	P_i	K	G_{ARX}, dB	P_{ARX}, deg	G_{ERA}, dB	P_{ERA}, deg
0.0001	−48.8	(−0.0870, 41.8)	32.8	14	75/−156	−36	25
	(−0.0825, 35.4)	(−0.0773, 32.5)					
0.0005	(−0.0477, 37.9)	(−0.0099, 38.5)	58.9	16	70/−65	−30	11
	−27.2	(−0.241, 30.4)					
0.001	−381	(−0.0445, 39.9)	5.65	20	65/−70	−6	62
	(−0.0129, 39.5)	(−0.108, 37.4)					
		−5.02					

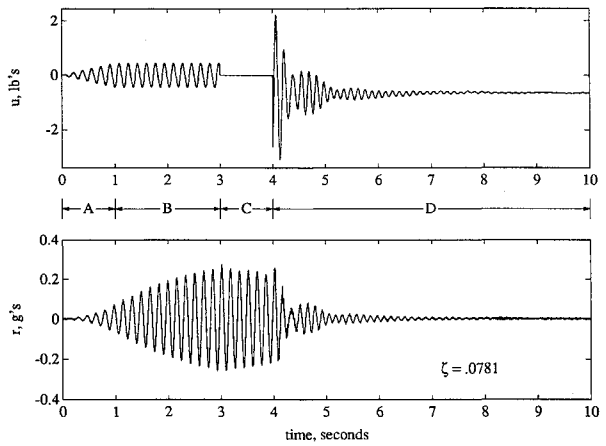

Fig. 8 Experimental results for μ synthesis design no. 1 with $\rho = 3$.

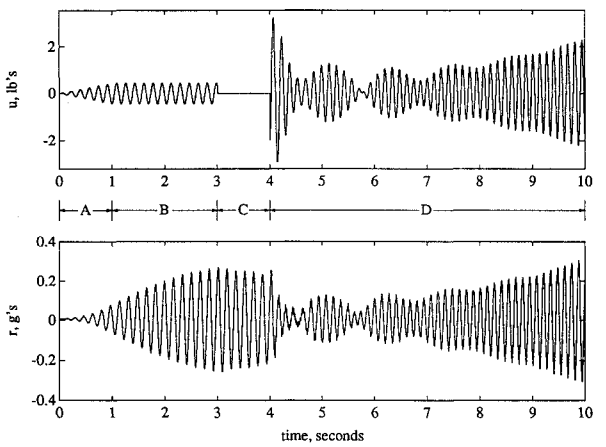

Fig. 9 Experimental results for μ synthesis design no. 2 with $\rho = 0.00313$.

Figures 5 and 6 present the experimental results for a ρ of 0.003 and 0.004 for the H_∞ compensators designs. In Fig. 5 the system response r decays. The H_∞ command response u, however, is exceeding the control limits (i.e., ±4.4 lbf) in the first two cycles. In Fig. 6 the system response is dominated by a constant amplitude oscillatory signal at 11 Hz. A root locus analysis is given in Fig. 7 for the ARX and the ERA plant models. The ERA analysis indicates that the out-of-plane bending mode will be unstable for all of the H_∞ compensators. The ERA analysis has the correct trend, but the estimated damping in the out-of-plane mode is lower than the true value. The effect is to predict the instability at a lower gain than is observed in the test. Figure 6 enforces the premise that H_∞ compensators are not robust.

μ Synthesis Designs

All of the μ synthesis compensators designed in this research were calculated using the procedures described by Doyle.[9-11] The design model for the μ synthesis compensators have two frequency-dependent functions added to the H_∞ design model. These functions are W_{unc}, the input uncertainty weighting, and W_{add}, the additional weighting. The weighting function W_{unc} describes the input uncertainty of the design model and is defined by the properties of the actuator. The W_{unc} is added to the design model as an additive uncertainty at the command input. The function W_{add} represents uncertainty that is added to the design model to control high-frequncy roll-off of the resulting compensator. The W_{add} is added to the design model as an additive uncertainty between the compensator output and plant output. The W_2 function in the H_∞ design model becomes the function W_{err} in the μ synthesis design model. The design parameters of the μ synthesis are the frequency-dependent functions W_{unc}, W_{add}, and W_{err}.

μ Synthesis Design No. 1

For the initial μ synthesis design, the input uncertainty was defined as

$$W_{unc} = \frac{s}{s+120}$$

The input uncertainty function is chosen such that the roll-off of the function is between the lower limit of the first bending mode, 5.8 Hz, and the upper limit of the actuator roll-off, 46 Hz. The additional uncertainty is defined as

$$W_{add} = \frac{25s}{s+7000}$$

The additive uncertainty function is chosen so that the resulting compensator had sufficient roll-off so as not to excite

the second bending mode of the 10-bay truss at 50 Hz but had sufficient bandwidth for the μ synthesis algorithm to generate an acceptable compensator. The error function W_{err} was changed from the W_2 function of the H_∞ to

$$W_{\text{err}} = \frac{\rho}{(s+1)} \frac{37^2}{\left[s^2+2(0.025)37s+37^2\right]}$$

to maintain a relatively flat frequency response of the resulting compensator. Table 4 gives the zeros, poles, gain, and margins for all of the compensators designed in this series.

μ Synthesis Design No. 1 Test Results

Figure 8 shows the time history test results of this μ synthesis controller. Note the large amount of residual force, 0.5 lbf, being commanded by the control law at $t = 10$ s. This is caused by the high static gain present in the control law. The value of μ for this compensator was 1.05. For values of $\mu < 1$, the compensator will meet the performance objective defined by W_{err} in the presence of the perturbations described by W_{unc} and W_{add}. Therefore, this compensator, with $\mu = 1.05$, would be slightly past the best performance level that could be obtained with the uncertainties specified by the parameters of the design model.

μ Synthesis Design No. 2

The second series of μ synthesis compensators are designed to reduce the high static gain obtained in the μ synthesis design no. 1 series. The error weight function was selected to be

$$W_{\text{err}} = \rho \frac{s}{(s+10)} \frac{37^2}{\left[s^2+2(0.025)37s+37^2\right]}$$

This modification widens the crossover region between the error function and the uncertainty functions. The additional weight was changed to

$$W_{\text{add}} = \frac{25s}{s+7000} + \frac{5}{s+5}$$

This change increases the uncertainty of the design model at low frequencies. The input uncertainty function W_{unc} was left unchanged. For this series of compensators, data for one value of ρ (0.00313) are presented. For this value of ρ, a value of $\mu = 0.52$ was obtained. Table 5 gives the poles, zeros, gain, and margins for this series of compensators. From the data in Tables 4 and 5, the objective of reducing the high static gain is shown to be achieved.

μ Synthesis Design No. 2 Test Results

Figure 9 presents the experimental results for the μ synthesis compensator design no. 2. This compensator has an unstable mode at 7.5 Hz. This compensator is unstable because the performance requirements were set too high while the differences between the 10-bay structure and the design model were large enough to cause the instability.

μ Synthesis Design No. 3

This series of μ synthesis compensators was designed to incorporate the uncertainty of the modal frequency of the assumed plant dynamics. The uncertainty of the design model can be estimated by noting the differences between the ARX and the ERA plant model. The differences of the squared frequency predictions of the two plant models is 20 (rad s^{-2}) for the in-plane mode and 2100 (rad s^{-2}) for the out-of-plane mode. These frequency uncertainties were incorporated into the design model for the final series of μ compensators. Because of the increased uncertainty of the design model, the error weight function used was changed to

$$W_{\text{err}} = \rho \frac{37^2 s}{s^2+2(0.025)37s+37^2}$$

and the additional weight was changed to

$$W_{\text{add}} = \frac{0.1}{s+0.1} + \frac{10s}{s+10000}$$

The input uncertainty function W_{unc} was left unchanged. There are only two compensators presented in this series, $\rho = [10^{-4}, 10^{-3}]$. The compensator for $\rho = 10^{-4}$ resulted in $\mu = 1.1$, and the compensator for $\rho = 10^{-3}$ resulted in $\mu = 1.3$. Since values of $\mu > 1$ indicate that the performance of the closed-loop system could not be achieved with the level of uncertainty specified, these compensators are expected to have stability problems if the uncertainty is correctly modeled. Table 6 gives the poles, zeros, gain, and margins for this series of compensators.

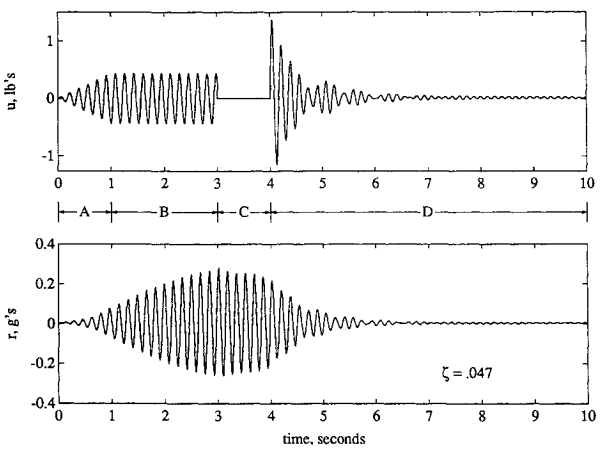

Fig. 10 Experimental results for μ synthesis design no. 3 with $\rho = 0.0001$.

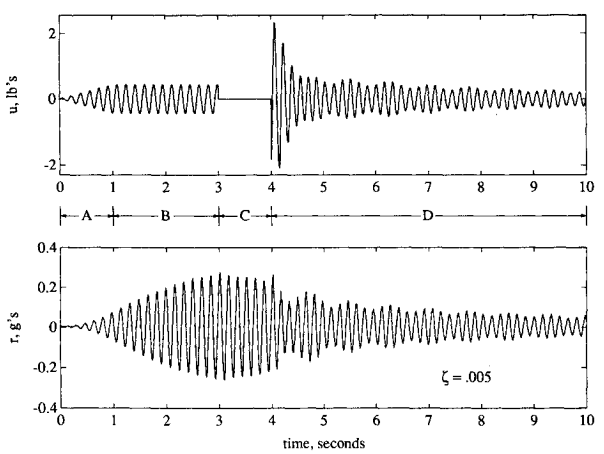

Fig. 11 Experimental results for μ synthesis design no. 3 with $\rho = 0.001$.

μ Synthesis Design No. 3 Test Results

Figures 10 and 11 present the experimental results for the μ synthesis compensator design no. 3. The experimental data show the response to have a critical damping of $\zeta = 0.047$ at $\rho = 0.0001$ and to be lightly damped at $\rho = 0.001$. These test results indicate that the μ compensators for $\rho = 0.0001$ are at the maximum level of performance for the series, and the uncertainty parameters specified in the design model are correct.

Summary and Conclusions

A series of active control compensators, designed with linear quadratic Gaussian/loop transfer recovery, H_∞, and μ synthesis methods, were tested to investigate the use of active control methods to suppress spacecraft structural vibration. The tests were used to qualify the advantages and disadvantages of the design methods in the presence of uncertainties. The linear quadratic Gaussian/loop transfer recovery methodology achieved the highest level of damping. The H_∞ method achieved the second highest damping level. The μ synthesis achieved the lowest damping increase of the compensators at about half that achieved with the linear quadratic Gaussian/loop transfer recovery method. All compensators had at least ± 6 dB gain and ± 60 deg of margin with respect to the design model. The H_∞ and μ compensators had instabilities that were not predicted by the methodologies. The H_∞ compensators were shown not to be robust in the presence of uncertainties. The μ synthesis compensators were shown to be robust only with respect to the uncertainty models that were used in their design. If the uncertainty specifications are not correct, then a μ synthesis compensator can become unstable.

References

[1]Juang, J.-N., Phan, M., Horta, L. G., and Longmann, R. W., "Identification of Observer/Kalman Filter Markov Parameters: Theory and Experiments," *Proceedings of the AIAA Guidance, Navigation, and Control Conference* (New Orleans, LA), AIAA, Washington, DC, 1991, pp. 1195–1207.

[2]Ljung, L., *System Identification—Theory for the User,* Prentice-Hall, Englewood Cliffs, NJ, 1987.

[3]Ljung, L., *System Identification Toolbox User's Guide,* The Math Works, Inc., Natick, MA, 1988.

[4]Harvey, C. A., Stein, G., and Doyle, J. C., "Optimal Linear Control (Characterization of Multi-Input Systems)," Office of Naval Research, ONR Rept. CR215-238-2, Arlington, VA, Aug. 1977.

[5]Doyle, J. C., and Stein, G., "Robustness with Observers," *IEEE Transactions on Automatic Control,* Vol. AC-24, No. 4, 1979, pp. 607–611.

[6]Doyle, J. C., and Stein, G., "Multivariable Feedback Design: Concept for a Classical/Modern Synthesis," *IEEE Transactions on Automatic Control,* Vol. AC-26, No. 1, 1981, pp. 4–16.

[7]Francis, B. A., Helton, J. W., and Zames, G., "H^∞-Optimal Feedback Controllers for Linear Multivariable Systems," *IEEE Transactions on Automatic Control,* Vol. AC-29, No. 10, 1984, pp. 888–899.

[8]Doyle, J. C., Glover, K., Khargonekar, P. P., and Francis, B. A., "State-Space Solutions to Standard H_2 and H_∞ Control Problems," *IEEE Transactions on Automatic Control,* Vol. AC-34, No. 8, 1989, pp. 831–847.

[9]Doyle, J. C., "Synthesis of Robust Controllers and Filters," *Proceedings of the IEEE Conference on Decision and Control* (San Antonio, TX), Inst. of Electrical and Electronics Engineers, New York, 1983, pp. 109–114.

[10]Doyle, J. C., "Structured Uncertainty in Control System Design," *Proceedings of the IEEE Conference on Decision and Control* (Fort Lauderdale, FL), Inst. of Electrical and Electronics Engineers, New York, 1985, pp. 260–265.

[11]Doyle, J. C., "A Review of μ for Case Studies in Robust Control," *1987 International Federation of Automatic Control Triennial World Congress* (Munich, Germany), Pergamon, New York, 1987, pp. 395–402.